Received: 1 May 2022 | Revised: 9 August 2022 | Accepted: 15 August 2022

DOI: 10.1002/mgg3.2043

Molecular Genetics & Genomic Medicine Open Access WILEY

ORIGINAL ARTICLE

Clinical characteristics of 10 Chinese patients with melorheostosis and identification of a somatic MAP2K1 variant in one case

Xiaojun Han[1] | **Yang Xu**[2] | **Zhanying Wei**[2] | **Chun Wang**[2] | **Hua Yue**[2] | **Zhenlin Zhang**[2]

[1]Department of Orthopedics, Qingpu Branch of Zhongshan Hospital Affiliated to Fudan University, Shanghai, China

[2]Shanghai Clinical Research Center of Bone Disease, Department of Osteoporosis and Bone Disease, Shanghai Jiao Tong University Affiliated Sixth People's Hospital, Shanghai, China

Correspondence
Hua Yue and Zhenlin Zhang, Shanghai Clinical Research Center of Bone Disease, Department of Osteoporosis and Bone Disease, Shanghai Jiao Tong University Affiliated Sixth People's Hospital, Shanghai 200233, China.
Email: yueyinglonghua@163.com (H. Y.) and zhangzl@sjtu.edu.cn (Z. Z.)

Funding information
Clinical Science and Technology Innovation Project of Shanghai Shenkang Hospital Development Center, Grant/Award Number: SHDC12018120; National Key Research and Development Program of China, Grant/Award Number: 2018YFA0800801; Shanghai Key Clinical Center for Metabolic Disease, Shanghai Health Commission Grant, Grant/Award Number: 2017ZZ01013; the National Natural Science Foundation of China, Grant/Award Number: 81770871, 81770872, 81770874 and 81974126

Abstract

Background: Melorheostosis (MEL) is an exceptionally rare sclerosing bone dysplasia with asymmetrically exuberant bone formation and soft tissue lesions in a segmental distribution. We aimed to summarize the clinical characteristics of Chinese MEL patients and identify their pathogenic cause.

Methods: In total, 10 Chinese MEL patients were recruited, and clinical manifestations and radiological characteristics were recorded. Sanger sequencing of the *LEMD3* gene was performed on peripheral blood samples of all patients, while the exome sequencing of matched peripheral blood, melorheostotic bone, and skin lesion samples was conducted on one patient who provided affected bone and skin tissues. Micro-computed tomography (micro-CT) was also used to scan the melorheostotic bone tissue.

Results: We found the average age of the 10 MEL patients was 29.5 years (range 11–40 years), and the major symptoms were bone pain, restricted movement, and bone deformity. The lesions sites were mainly located in femur (8/10), tibia (8/10), fibula (6/10), and foot (7/10), the next was pelvis (4/10), and the last were patella (1/10), hand (1/10) and spine (1/10). Radiological examinations showed a mixture of hyperostosis consisting of classic "dripping candle wax," "osteoma-like," or "myositis ossificans-like" patterns in most patients. No germline pathogenic variants in the *LEMD3* gene were found in all patients, but a disease-causing somatic variant of *MAP2K1* (c.167A > C, p.Gln56Pro) was detected in melorheostotic bone from one patient. Moreover, the micro-CT analysis showed increased porosity in the melorheostotic bone with somatic *MAP2K1* variant.

Xiaojun Han and Yang Xu contributed equally to this work.

Conclusion: This is a summary of the clinical characteristics of Chinese MEL patients and we first identify the somatic *MAP2K1* variant in Chinese patients. Our findings validate the molecular genetic mechanism of MEL and broaden its phenotype spectrum in the Chinese population.

KEYWORDS

exome sequencing, *MAP2K1*, Melorheostosis, micro-CT, somatic variant

1 | INTRODUCTION

Melorheostosis (MEL, OMIM 155950) is a sclerosing bone disease characterized by hyperostotic lesions in a "dripping candle wax" pattern on the cortex of the long tubular bones (Freyschmidt, 2001). It is a sporadic disease occurring in males and females equally, and the low prevalence of 1/1,000,000 makes MEL rare (Kotwal & Clarke, 2017; Wynne-Davies & Gormley, 1985). MEL lesions are asymmetrically distributed, often with multiple contiguous bones involved. Although the involvement of one limb is typical, more widespread involvement is not uncommon (Kotwal & Clarke, 2017; Smith et al., 2017; Wordsworth & Chan, 2019). Although the overgrowth lesions of MEL do not metastasize, the malignant change to osteosarcoma has been reported (Bostman et al., 1987; Murphy et al., 2003). Abnormalities of the adjacent soft tissues may result in sensory deficits, linear epidermal nevus (LEN), scleroderma-like skin (SLS), subcutaneous fibrosis, ectopic bone formation, and fibrolipmas accompany (Hellemans et al., 2004). Despite the absence of definitive diagnostic criteria, patients with MEL can usually be recognized from a combination of clinical findings, radiographs, and bone scans (Kotwal & Clarke, 2017).

The majority of MEL cases are isolated but a minority occur against a background of other hyperostotic bone diseases, osteopoikilosis (OPK, OMIM 166700) and Buschke-Ollendorff syndrome (BOS, OMIM 166700), two benign disorders caused by germline variants in the *LEMD3* gene (OMIM 607844) (Hellemans et al., 2004). *LEMD3* encodes the inner nuclear membrane protein MAN1, an antagonist in the TGF-β/BMP signaling pathway (Lin et al., 2005). The germline variant of *LEMD3* accompanied by heterozygous somatic *KRAS* (OMIM 190070) variant was identified as the cause of the SLS lesion in a patient with MEL and familial OPK (Whyte et al., 2017). In patients with isolated MEL, no pathogenic germline *LEMD3* variants were identified, but somatic activating variants in *MAP2K1* (OMIM 176872), encoding MEK1 kinase, were found by comparing the exome sequences of affected and unaffected tissues (Mortier et al., 2019; Mumm et al., 2007). In addition to disease-causing variants in the negative regulatory domain of MEK1 kinase (p.Gln56Pro, p.Lys57Glu, and p.Lys57Asn), which were proved to increase enzymatic activity and phosphorylation of extracellular signal-regulated kinase (ERK), the variant in the catalytic domain (p.Cys121Ser) was also identified as associated with MEL (De Ridder et al., 2020; Kang et al., 2018). Furthermore, somatic activating variants in *SMAD3* (OMIM 603109) were also discovered to cause MEL by up-regulating the TGF-β/SMAD pathway (Kang et al., 2020). So far, the etiology and molecular pathogenesis of MEL have been preliminarily elucidated. However, no Chinese MEL patients with definite genetic diagnoses were reported and no clear summary of the clinical characteristics of Chinese MEL patients was made.

In this study, we investigated 10 Chinese MEL patients diagnosed with clinical manifestations and typical radiological findings. Through Sanger sequencing on the *LEMD3* gene of all the patient's peripheral blood samples and exome sequencing on the biopsied melorheostotic bone and skin lesion tissues of one case, we identified a pathogenic somatic variant in *MAP2K1* for the first time in a Chinese MEL patient.

2 | MATERIALS AND METHODS

2.1 | Ethical compliance

The present study was reviewed and approved by the Ethics Committee of the Shanghai Jiao Tong University Affiliated Sixth People's Hospital, and written informed consent were obtained from all the patients and the healthy volunteer.

2.2 | Subjects

Ten sporadic MEL patients of Han ethnicity were recruited in our outpatient from August 2009 to June 2018. The patients were diagnosed with MEL according to their clinical manifestations, plain radiography, and some even radionuclide bone scan. The principal characteristics of these patients were listed in Table 1.

Among the patients, patient 10 first came to our department in February 2013. She was born to a healthy non-consanguineous couple. From 30 years old, restricted motion range of the left hip, knee, and ankle made the patient limp, and at 37 years old, she came to our department for severe pain in the above joints. Physical examination revealed mild scoliosis, bilateral lower extremities asymmetry, and hard lumps around the left popliteal fossa and ankle. A large cutaneous lesion with prominent brown macules and erythema extended from her posterior waist to left thigh and leg following Blaschko lines.

2.3 | Blood and tissue sampling

Peripheral blood (2 ml) was obtained from all 10 patients for genomic DNA extraction. Patient 10, underwent open surgery to remove hyperplastic and sclerosing bone tissues, which restricted her motion, in our hospital. The excised bone and lesional skin tissue were immediately placed in liquid nitrogen for DNA extraction or 4% paraformaldehyde for micro-CT. The control bone sample with no radiographic evidence of MEL was obtained from the proximal tibia of a middle-aged female patient who underwent amputation surgery after a car accident. Unfortunately, the remaining 9 patients with MEL were not operated on at our hospital, so we were unable to obtain their affected bone or skin tissues.

2.4 | Exome sequencing and sanger sequencing

Genomic DNA was extracted from 10 blood, two bone samples, and one skin lesion tissue using QuickGene DNA whole-blood Kit (Kurabo Industries Ltd., Osaka, Japan) and Qiagen DNeasy tissue Kit (Qiagen, Venlo, The Netherlands).

First, Sanger sequencing on the *LEMD3* gene was performed on the 10 patients. All exons and the exon-intron boundaries of the *LEMD3* gene (GenBank accession No. NM_014319.4) were amplified via polymerase chain reaction (PCR) using the primers designed by Primer 3 software (http://frodo.wi.mit.edu/primer3/). Direct nucleotide sequencing of the amplicons was performed using the BigDye Terminator Cycle Sequencing Ready Reaction Kit (version 3.1; Thermo Fisher Scientific, Inc., Waltham, USA) and analyzed by an ABI 3130 automated sequencer (Thermo Fisher Scientific, Inc., Waltham, USA).

Exome sequencing was applied to genomic DNA isolated from matched blood, bone, and skin samples of Patient 10. All samples were fragmented into 100–800 bp pieces with a peak size of ~250 bp via NEBNext dsDNA Fragmentase (New England Biolabs, Ipswich, UK). And then, end-repairing, dA-Tailing, and adaptor ligation were conducted using the NEBNext DNA Library Prep Reagent Set from Illumina (New England Biolabs, Ipswich, UK). 2% agarose gel electrophoresis was used to fraction adaptor-ligated DNA fragments and fragments of the desired size (300–400 bp) were excised. 10 PCR cycles were adopted to amplify the extracted DNA with PE primers (Illumina, San Diego, USA) and Phusion DNA polymerase (New England Biolabs, Ipswich, UK). The PCR products were then subjected to exome sequence capture using the SureSelect Human All Exon V6 (Agilent, Santa Clara, USA). The amplicons were size-checked and quantitated using a BioAnalyzer 2100 (Agilent, Santa Clara, USA), and then subjected to 2×150 bp paired-end massively parallel sequencing using a Hiseq2000 Sequencing System (Illumina, San Diego, USA). After filtering out the candidate pathogenic variants by comparing the exome sequencing data of blood, bone, and skin tissue, validation was conducted with Sanger sequencing again.

2.5 | Micro-CT of bone tissues

The biopsied bone from patient 10 with MEL and corresponding control bone tissue from the volunteer were analyzed by SkyScan 1176 (Bruker MicroCT, Kontich, Belgium) operated at 65 kV with a 0.5 mm Al filter and 520 ms exposure time per projection. The scanning was captured at 0.35 degrees over a total of 180 degrees. The 1.6 version of NR econ software was used for 3D reconstruction and image viewing. Then, the segmentation was performed with the range from 20/130 to 120/255, and after segmentation, the inverted images were used to obtain the bone mass and pores. The parameters of bone mass include BMD (mg/cm^3) and percent bone volume (BV/TV, %), and properties of pores including percent pore volume (Po.V/TV, %), pore diameters (Po.Dm, mm) and pore number (Po.N, 1/mm), were calculated in a cubic (1.2 mm*1.2 mm*1.2 mm) region of interesting (ROI) by CTan software (Bruker MicroCT, Kontich, Belgium). Three cubic regions in normal bone tissue and six cubic regions in biopsied osteophytes were selected for statistical analysis. The 3D rendering of the bones and pores was performed using CTvox software (Bruker MicroCT, Kontich, Belgium).

3 | RESULTS

3.1 | Clinical features

Table 1 listed the clinical features of the 10 sporadic MEL patients. There were 4 men and 6 women with an average age of 29.5 years (range 11–40 years), and the average age at symptoms onset was 21.2 years (range 10–38 years).

TABLE 1 Clinical features of the ten MEL patients in this study

Patient	Gender	Age (years)	Affected side	Affected sites	Age at symptom onset (years)	Symptoms and signs	Radiographic pattern	Skin lesions	Bone scan
1	Male	27	Right	Pelvis, femur, tibia, fibula, foot	12	Enlarged right lower extremity, bone pain	Mixed (classic+ osteoma-like+ myositis ossificans-like)	−	+
2	Female	40	Left	Tibia, fibula	38	Tibia protrusion, bone pain	Classic	−	+
3	Male	32	Right	Femur, patella, tibia	16	Tibia protrusion, bone pain, restricted movement	Mixed (classic+ osteoma-like)	−	NT
4	Female	22	Left	Pelvis, femur, tibia, fibula, foot	12	Lower extremity deformity, restricted movement	Classic	−	NT
5	Female	36	Right	Femur, tibia, foot	33	Bone pain, restricted movement	Mixed (classic+ osteoma-like)	−	NT
6	Male	32	Right	Hand	22	Bone pain	Mixed (classic+ osteoma-like)	−	NT
7	Male	11	Right	Femur, tibia, fibula, foot	10	Bone pain	Mixed (classic+ osteoma-like)	−	NT
8	Female	27	Left	Pelvis, femur, tibia, fibula, foot	17	Bone pain	Mixed (classic+ osteoma-like)	Scleroderma-like skin	+
9	Female	31	Left	Femur, foot	22	Bone pain	Mixed (classic+ myositis ossificans-like)	−	NT
10[a]	Female	37	Left + spine	Spine, pelvis, femur, tibia, fibula, foot	30	Bone pain, restricted movement	Mixed (classic+ osteoma-like+ myositis ossificans-like)	Scleroderma-like skin, linear epidermal nevus	+

Abbreviations: NT, not tested; +, present; −, not present.

[a]A 37-year-old female who carries a somatic p.Gln56Pro variant of the *MAP2K1* gene in affected bone tissue.

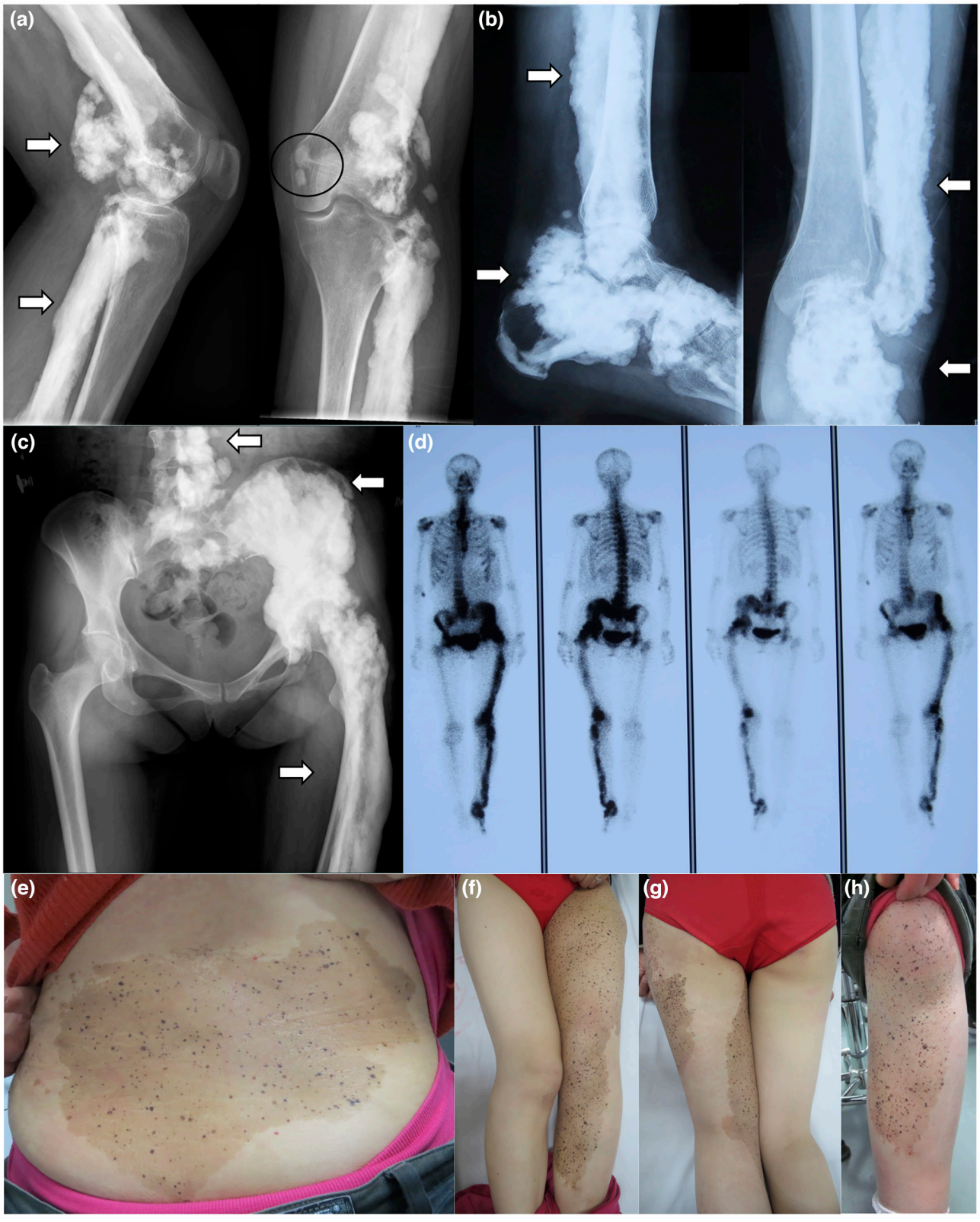

FIGURE 1 Radiographs, bone scintigraphy, and photographs of patient 10. (a) X-rays of the left knee joint show a "dripping candle-wax" appearance of hyperostosis in the left fibula, "myositis ossificans-like" pattern in the vicinity of the joint, "osteoma-like" hyperostosis in the endosteal surface of the left femur. (b) Radiographs of the left ankle joint reveal melorheostotic lesions in the left fibula, calcaneus, talus, navicular, cuboid, and cuneiforms. (c) X-rays of the pelvis demonstrated a "dripping candle-wax appearance" of MEL in L4, L5, left ilium, and periosteal and endosteal surfaces of the cortex of the left femur. (d) Bone scintigraphy displays larger areas than that shown by X-rays. (e–h) a classic linear epidermal nevus and scleroderma-like skin lesions extend from the patient's posterior waist to the left thigh and leg following Blaschko lines

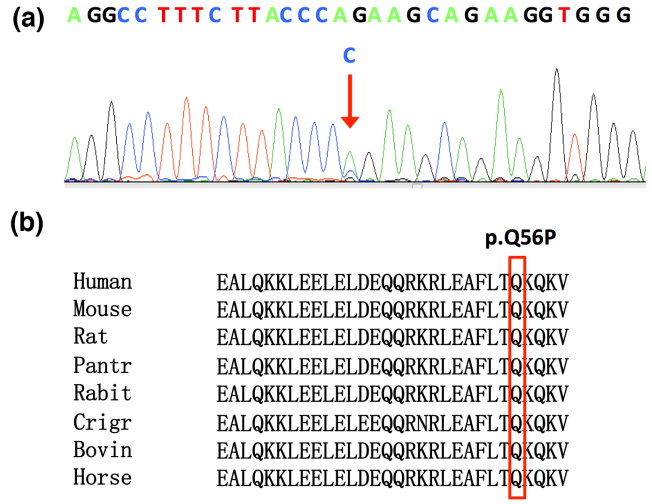

FIGURE 2 Sanger sequencing and conservation analysis. (a). The heterozygous missense variant, p.Gln56Pro (c.167A > C) in exon 2 of *MAP2K1*, is found in the affected bone tissue of the Chinese patient with MEL. (b). p.Gln56 is evolutionarily highly conserved among eight vertebrates

The disease manifested clinically with bone pain, restricted movement, and bone deformities. In the 10 patients, MEL lesions were involved with multiple contiguous bones unilaterally: the lesion sites were mainly located in the lower extremity, including femur (8/10), tibia (8/10), fibula (6/10), and foot (7/10), the next was pelvis (4/10), and the last were patella (1/10), hand (1/10), and spine (1/10). X-ray imaging revealed bony changes consistent with MEL, in which, 2 patients showed the classic MEL feature, namely "dripping candle wax" appearance of hyperostosis in periosteal or endosteal bone surfaces, 5 displayed a mixed pattern of "classic" and "osteoma-like" hyperostosis, and the remaining 3 manifested with a more complicated mixed pattern of "classic", "osteoma-like" and "myositis ossificans-like" hyperostosis. 4 patients underwent a radionuclide bone scan, and all skeletal melorheostotic abnormalities demonstrated intensely elevated ^{99m}Tc-MDP uptake. Among all the patients, patient 10 had the most extensive bone involvement and relatively heavy disease burden (Figure 1). In addition to bone lesions, 2 patients also presented skin lesions. Patient 8 displayed a small SLS lesion in the anterior tibia, while patient 10 had a large cutaneous lesion, including LEN and SLS lesion, extended from her posterior waist to left thigh and leg following Blaschko lines (Figure 1).

3.2 | Identification of somatic variant in *MAP2K1*

After Sanger sequencing on the *LEMD3* gene, no pathogenic variants were found in the genomic DNA from peripheral blood samples of the 10 MEL patients. Then, exome sequencing was conducted on genomic DNA isolated from matched blood, biopsied bone, and skin samples of patient 10. sequence alignment files were generated to duplicate removal, local realignment, and base quality recalibration with the Genome Analysis Toolkit (GATK). Variations including single-nucleotide variants (SNVs) and small insertions or deletions (Indels) were identified with variant quality score recalibration (VQSR). Then, SNVs with a minor allele frequency of <1% in the Chinese 1000 genome database and SIFT score of <0.05, Polyphen-2 score of >0.85, or MutationTaster score of >0.85 were considered as significant of not being benign. According to the above restrictions and comparison among blood, bone, and skin tissues, somatic variants were filtered from those that were present in the affected bone or skin tissue, but not present in the blood, and caused protein changes or splicing changes. Finally, the somatic missense variant in exon 2, the coding region of *MAP2K1* (GenBank accession No. NM_002755.3), c.167A > C (p.Gln56Pro), causing amino acid substitution of glutamine to proline in the protein MEK1, was identified in the bone tissue of Patient 10 (Figure 2). However, no pathogenic somatic variants in *MAP2K1* or other genes were found in the skin lesion tissue. The *MAP2K1* variant, p.Gln56Pro, occurred at a conserved position in eight vertebrates based on Universal Protein Resource (Figure 2). The above *MAP2K1* variant was then verified by Sanger sequencing to be absent in the control bone sample from the volunteer. Since we were unable to obtain the affected bone or skin tissues of the remaining 9 patients, we could not determine whether they carried pathogenic somatic variants in the *MAP2K1* gene or other genes through exome sequencing.

3.3 | Micro-CT of bone tissues

To explore the microstructures of bone with melorheostotic lesions, micro-CT with a resolution of 8.96 um was adopted to scan the osteophytes biopsied from Patient 10 and unaffected bone samples obtained from the volunteer, respectively. The 2D radiographies of micro-CT showed homogeneously dense cortical tissue with consistently sized pores in unaffected bone tissue, but increased pores with larger size were found in biopsied affected osteophytes with *MAP2K1* variant (Figure 3). The 3D renderings segmented the calcified tissue and vascular pores, and clearly showed decreased bone volume and elevated porosity in the biopsied osteophytes (Figure 3). Quantitatively, BMD and percent bone volume (BV/TV) was decreased in affected bone versus unaffected bone. In addition, the increased porosity in affected bone was manifested with elevated percent pore volume (Po.V/TV), pore

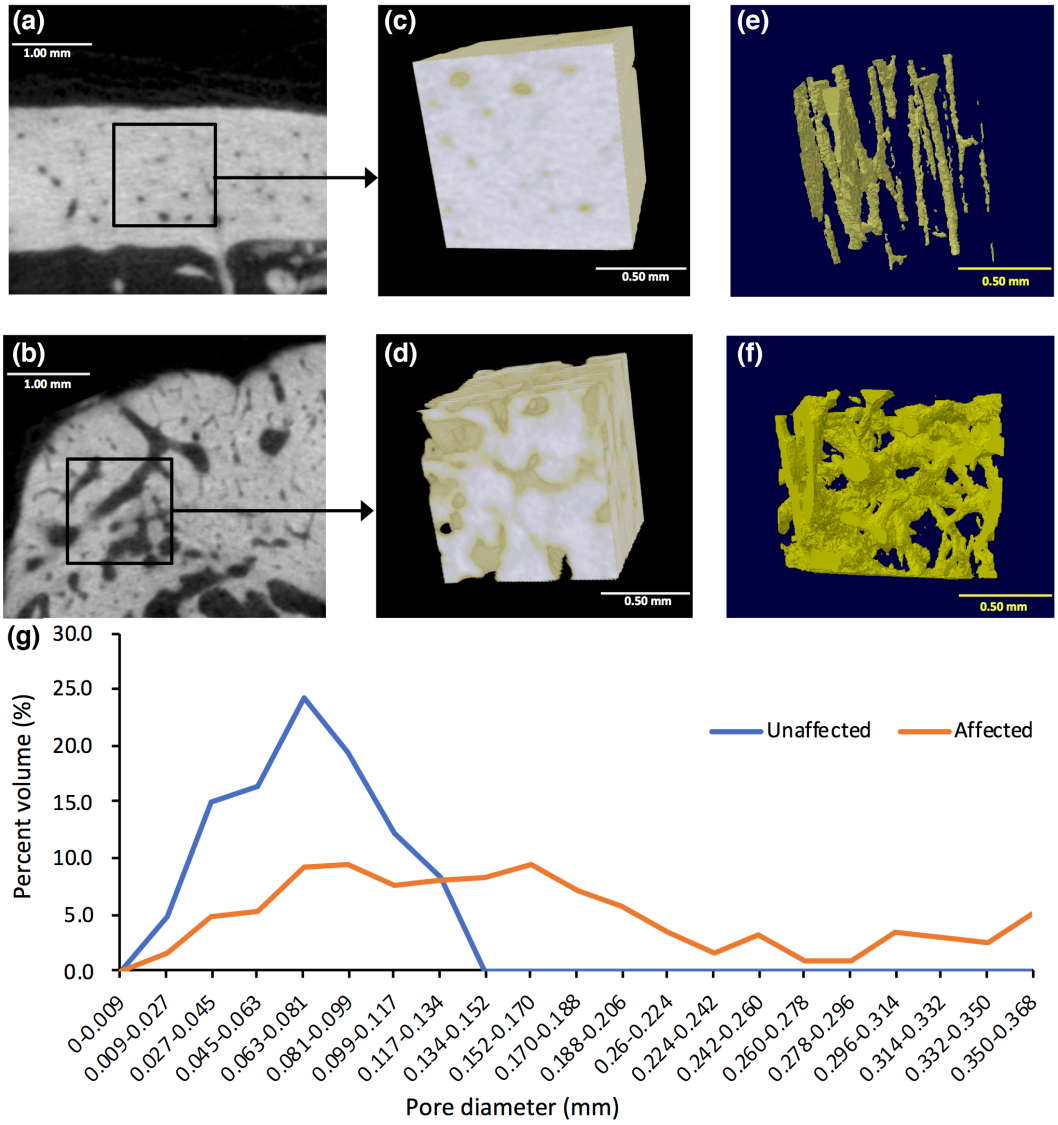

FIGURE 3 Micro-CT evaluations of bone tissues. (a) 2D radiography of unaffected bone shows homogeneously dense cortical tissue. (b) 2D radiography of affected bone displays increased pores with the larger size. (c and e) 3D rendering of unaffected bone reveals normal bone volume and porosity. (d and f) 3D rendering of affected bone demonstrates the decreased bone volume and elevated porosity. (g) the curve diagram of the contribution of pore size to percent pore volume shows a notably wider range of pore diameters in the affected bone

TABLE 2 Comparison of microstructure characteristics between melorheostotic and unaffected bone tissues

	Unaffected	Affected	*p*-value
BMD (g/cm^3)	0.740 ± 0.001	0.673 ± 0.022	.002**
BV/TV (%)	94.44 ± 2.25	76.41 ± 8.80	.012*
Po.V/TV (%)	5.72 ± 2.27	23.91 ± 8.91	.012*
Po.Dm (mm)	0.071 ± 0.013	0.141 ± 0.012	<.001**
Po.N (/mm)	0.781 ± 0.185	1.676 ± 0.573	.037*

Abbreviations: BMD, bone mineral density; BV/TV, percent bone volume; Po.Dm, pore diameters; Po.N, pore numbers; Po.V/TV, percent pore volume.
*$p < .05$;; **$p < .01$.

diameters (Po.Dm), and pore numbers (Po.N) versus unaffected bone (Table 2). The pore diameters also showed significantly different distributions (Figure 3). In unaffected bone, the maximum pore diameter was 0.134 mm, while the range of pore diameters was notably wider with the maximum pore diameter of 0.368 in affected bone tissue. The results showed significantly increased porosity due to increased tissue vascularity in the affected bone tissue.

4 | DISCUSSION

With the progress of research, the molecular pathogenesis of MEL is gradually revealed. In the majority of sporadic MEL cases, the causal somatic variants in *MAP2K1* and *SMAD3* are identified from melorheostotic bone (De Ridder et al., 2020; Kang et al., 2018). Most variants in the *MAP2K1*, cluster in the negative regulatory domain of

TABLE 3 Comparison of clinical features between ten Chinese sporadic MEL patients and those in Mayo Clinic

	MEL in this study	MEL in Mayo Clinic
Age (years)	Average 29.5	Average 36.5
Gender predilection (male to female ratio)	2:3	1:4
Symptoms and signs	Bone pain (90%), restricted movement (40%), deformity (40%)	Pain (83.3%), deformity (54.2%), limitation of motion (45.8%), numbness (37.5%), weakness (25.0%)
Affected sites	Femur (80%), tibia (80%), foot (70%), fibular (60%), pelvis (40%), patella (10%), hand (10%), spine (10%)	Leg (66.7%), ankle or foot (37.5%), hand or wrist (29.1%), arm (33.3%), spine (16.6%), head (8.3%)
Unilateral limbs involvement	90%	83%
Average number of affected sites per patient	3.6	4.4

MEK1 (p.Gln56Pro, p.Lys57Glu, and p.Lys57Asn), causing loss of inhibitory effect, activating MEK1 in the RAS signaling pathway and following increasing phosphorylation of ERK, which promote osteoblast proliferation and reduce their differentiation. A novel variant (p.Cys121Ser) in the catalytic domain is also identified as associated with MEL (De Ridder et al., 2020). In some *MAP2K1*-negative cases, somatic *SMAD3* variants are identified, which upregulate the TGF-β/SMAD pathway (Kang et al., 2018; Kang et al., 2020). In MEL cases that appeared based on OPK or BOS, germline deactivating variants in *LEMD3* influence the negative regulation of MAN1 on SMAD transcription factors in TGF-β/BMP superfamily signaling (Couto et al., 2007; Hellemans et al., 2004). Somatic variant in *KRAS* located upstream of the RAS signaling pathway was also detected in the SLS of a case with polyostotic MEL and familiar OPK caused by germline *LEMD3* variant (Whyte et al., 2017). This may implicate variants in the RAS signaling pathway can be the "second hit" upon the *LEMD3* haploinsufficiency, and abnormalities in RAS and TGF-β signaling pathways lie at the pathogenic heart of MEL. Considerable crosstalk between RAS and TGF-β signaling and *RUNX2* activation via MAPK and PI3K/AKT pathway made the mechanism of MEL more complicated and attractive (Cohen-Solal et al., 2015; Grusch et al., 2010; Vivekanandhan & Mukhopadhyay, 2019). In this study, we failed to find pathogenic germline variants in *LEMD3* in any of the ten MEL patients, but a somatic *MAP2K1* (p.Gln56Pro) variant was identified in the bone lesion of one patient. However, no pathogenic somatic variants in *MAP2K1* or other genes were found in the skin lesion tissue of the same patient. Unfortunately, we were unable to collect the affected bone and skin tissues of the remaining 9 patients, since they did not undergo relevant surgery in our hospital. The difficulty of obtaining bone and skin samples may be a big obstacle to detect somatic variants. To the best of our knowledge, this is the first report of a Chinese MEL patient carrying a somatic *MAP2K1* variant, which is a rare but apparently specific invariant for MEL. The finding may further confirm the pathogenicity of somatic *MAP2K1* variants and validate the molecular mechanism of MEL in Chinese patients.

In Table 3, the clinical features of ten Chinese MEL patients were summarized and compared with those in the largest published clinical review about MEL in Mayo Clinic (Smith et al., 2017). The average age of our patients seems to be younger, and the male-to-female ratio seems to be higher. Concordant with Mayo Clinic's findings, we found recurrent pain, movement limitation, and limb deformity were the major presenting concerns, but numbness and weakness were not observed in our patients (Smith et al., 2017). MEL is typically limited to one limb but more widespread involvement is not unusual (Wordsworth & Chan, 2019). Unilateral limb involvement was present in 90% of our cases, and the affected lesions were contiguous and often crossed joint lines. Among all sites, appendicular skeleton especially lower extremities including femur, tibia, fibula, and foot were more commonly affected, while axial skeleton including skull and vertebrae was rare. The average number of affected sites per patient of 3.6 was similar to that of 4.4 in the Mayo cohort. In addition to classic "dripping candle wax" radiological features, three other radiologic presentations have also been described about MEL: (1) "osteoma-like" hyperostosis, which involved the endosteal surface and orientated in the long axis of the affected bone, (2) "osteopathia striata-like" hyperostosis, showing unilateral, long and dense striations near the inner surface of the cortex, (3) "myositis ossificans-like" pattern, with or without intraosseous hyperostosis

(Freyschmidt, 2001). In our study, most cases displayed a mixture of one or more of the above patterns, which may confuse the diagnosis of MEL with OPK, BOS, and osteopathia striata (Ethunandan et al., 2004; Gnoli et al., 2019; Ihde et al., 2011; Mumm et al., 2007; Zhang et al., 2009). The microstructure of melorheostotic lesion showed two strikingly different regions including the outer periosteal apposition (PA) tissue with little porosity and deeper osteonal remodeling (OR) bone with more porosity according to Fratzl-Zelman et al. (2019). In this study, Micro-CT of "myositis ossificans-like" bone biopsied from the patient showed significantly increased porosity with increased tissue vascularity in OR bone, however, no PA region was observed, which may be due to differences in hyperostosis types and biopsy locations. Moreover, consistent with the literature, a large area of LEN and SLS were observed overlying the affected bones in the female patient (Jha et al., 2019; Rhys et al., 1998; Woolridge et al., 2005).

5 | CONCLUSION

To conclude, this is a summary of clinical features of Chinese MEL patients and the first study to identify somatic *MAP2K1* variant in Chinese MEL patients. Our findings further validate the molecular genetic mechanism of MEL and broaden its phenotype spectrum in different populations.

AUTHOR CONTRIBUTIONS

Xiaojun Han, Yang Xu: Investigation, Formal analysis, Data collection, Writing-original draft; **Zhangying Wei:** Data collection; Formal analysis; **Chun Wang:** Funding acquisition, Supervision; **Hua Yue, Zhenlin Zhang:** Conceptualization, Funding acquisition, Supervision, Writing-review&editing. All authors read and approved the final version of the manuscript.

ACKNOWLEDGMENTS

We are grateful to all patients and healthy volunteer. We acknowledge technical assistance from Shanghai Genesky Bio-Teck Co., Ltd.

FUNDING INFORMATION

The study was supported by the National Key Research and Development Program of China (2018YFA0800801), Shanghai Key Clinical Center for Metabolic Disease, Shanghai Health Commission Grant (2017ZZ01013), the National Natural Science Foundation of China (NSFC) (81770872, 81770874, 81974126 and 81770871), and the Clinical Science and Technology Innovation Project of Shanghai Shenkang Hospital Development Center (SHDC12018120).

CONFLICT OF INTEREST

The authors declare no conflicts of interest.

DATA AVAILABILITY STATEMENT

The data that support the findings of this study are available from the corresponding author upon reasonable request.

ETHICS STATEMENT

This study was approved by the Ethics Committee of the Shanghai Jiao Tong University Affiliated Sixth People's Hospital, and written informed consent were obtained from all the patients and healthy volunteers. All methods were performed in accordance with the Declaration of Helsinki.

ORCID

Hua Yue https://orcid.org/0000-0002-9179-5894
Zhenlin Zhang https://orcid.org/0000-0002-4339-1617

REFERENCES

Bostman, O. M., Holmstrom, T., & Riska, E. B. (1987). Osteosarcoma arising in a melorheostotic femur. A case report. *The Journal of Bone and Joint Surgery. American Volume*, *69*(8), 1232–1237 https://www.ncbi.nlm.nih.gov/pubmed/3478336

Cohen-Solal, K. A., Boregowda, R. K., & Lasfar, A. (2015). RUNX2 and the PI3K/AKT axis reciprocal activation as a driving force for tumor progression. *Molecular Cancer*, *14*, 137. https://doi.org/10.1186/s12943-015-0404-3

Couto, A. R., Bruges-Armas, J., Peach, C. A., Chapman, K., Brown, M. A., Wordsworth, B. P., & Zhang, Y. (2007). A novel LEMD3 mutation common to patients with osteopoikilosis with and without melorheostosis. *Calcified Tissue International*, *81*(2), 81–84. https://doi.org/10.1007/s00223-007-9043-z

De Ridder, R., Boudin, E., Zillikens, M. C., Ibrahim, J., van der Eerden, B. C. J., Van Hul, W., & Mortier, G. (2020). A multi-omics approach expands the mutational spectrum of MAP2K1-related melorheostosis. *Bone*, *137*, 115406. https://doi.org/10.1016/j.bone.2020.115406

Ethunandan, M., Khosla, N., Tilley, E., & Webb, A. (2004). Melorheostosis involving the craniofacial skeleton. *The Journal of Craniofacial Surgery*, *15*(6), 1062–1065. https://doi.org/10.1097/00001665-200411000-00038

Fratzl-Zelman, N., Roschger, P., Kang, H., Jha, S., Roschger, A., Blouin, S., Deng, Z., Cabral, W. A., Ivovic, A., Katz, J., Siegel, R. M., Klaushofer, K., Fratzl, P., Bhattacharyya, T., & Marini, J. C. (2019). Melorheostotic bone lesions caused by somatic mutations in MAP2K1 have deteriorated microarchitecture and periosteal reaction. *Journal of Bone and Mineral Research*, *34*(5), 883–895. https://doi.org/10.1002/jbmr.3656

Freyschmidt, J. (2001). Melorheostosis: A review of 23 cases. *European Radiology*, *11*(3), 474–479. https://doi.org/10.1007/s003300000562

Gnoli, M., Staals, E. L., Campanacci, L., Bedeschi, M. F., Faletra, F., Gallone, S., Gaudio, A., Mattina, T., Gurrieri, F., Percesepe, A., Neri, I., Virdi, A., Tremosini, M., Milanesi, A., Brizola, E., Pedrini, E., & Sangiorgi, L. (2019). Melorheostosis and

Osteopoikilosis clinical and molecular description of an Italian case series. *Calcified Tissue International*, *105*(2), 215–221. https://doi.org/10.1007/s00223-019-00565-6

Grusch, M., Petz, M., Metzner, T., Ozturk, D., Schneller, D., & Mikulits, W. (2010). The crosstalk of RAS with the TGF-beta family during carcinoma progression and its implications for targeted cancer therapy. *Current Cancer Drug Targets*, *10*(8), 849–857. https://doi.org/10.2174/156800910793357943

Hellemans, J., Preobrazhenska, O., Willaert, A., Debeer, P., Verdonk, P. C., Costa, T., Janssens, K., Menten, B., Van Roy, N., Vermeulen, S. J. T., Savarirayan, R., Van Hul, W., Vanhoenacker, F., Huylebroeck, D., De Paepe, A., Naeyaert, J.-M., Vandesompele, J., Speleman, F., Verschueren, K., ... Mortier, G. R. (2004). Loss-of-function mutations in LEMD3 result in osteopoikilosis, Buschke-Ollendorff syndrome and melorheostosis. *Nature Genetics*, *36*(11), 1213–1218. https://doi.org/10.1038/ng1453

Ihde, L. L., Forrester, D. M., Gottsegen, C. J., Masih, S., Patel, D. B., Vachon, L. A., White, E. A., & Matcuk, G. R. (2011). Sclerosing bone dysplasias: Review and differentiation from other causes of osteosclerosis. *Radiographics*, *31*(7), 1865–1882. https://doi.org/10.1148/rg.317115093

Jha, S., Fratzl-Zelman, N., Roschger, P., Papadakis, G. Z., Cowen, E. W., Kang, H., Lehky, T. J., Alter, K., Deng, Z., Ivovic, A., Flynn, L., Reynolds, J. C., Dasgupta, A., Miettinen, M., Lange, E., Katz, J., Klaushofer, K., Marini, J. C., Siegel, R. M., & Bhattacharyya, T. (2019). Distinct clinical and pathological features of Melorheostosis associated with somatic MAP2K1 mutations. *Journal of Bone and Mineral Research*, *34*(1), 145–156. https://doi.org/10.1002/jbmr.3577

Kang, H., Jha, S., Deng, Z., Fratzl-Zelman, N., Cabral, W. A., Ivovic, A., Meylan, F., Hanson, E. P., Lange, E., Katz, J., Roschger, P., Klaushofer, K., Cowen, E. W., Siegel, R. M., Marini, J. C., & Bhattacharyya, T. (2018). Somatic activating mutations in MAP2K1 cause melorheostosis. *Nature Communications*, *9*(1), 1390. https://doi.org/10.1038/s41467-018-03720-z

Kang, H., Jha, S., Ivovic, A., Fratzl-Zelman, N., Deng, Z., Mitra, A., Cabral, W. A., Hanson, E. P., Lange, E., Cowen, E. W., Katz, J., Roschger, P., Klaushofer, K., Dale, R. K., Siegel, R. M., Bhattacharyya, T., & Marini, J. C. (2020). Somatic SMAD3-activating mutations cause melorheostosis by up-regulating the TGF-beta/SMAD pathway. *The Journal of Experimental Medicine*, *217*(5), e20191499. https://doi.org/10.1084/jem.20191499

Kotwal, A., & Clarke, B. L. (2017). Melorheostosis: A rare sclerosing bone dysplasia. *Current Osteoporosis Reports*, *15*(4), 335–342. https://doi.org/10.1007/s11914-017-0375-y

Lin, F., Morrison, J. M., Wu, W., & Worman, H. J. (2005). MAN1, an integral protein of the inner nuclear membrane, binds Smad2 and Smad3 and antagonizes transforming growth factor-beta signaling. *Human Molecular Genetics*, *14*(3), 437–445. https://doi.org/10.1093/hmg/ddi040

Mortier, G. R., Cohn, D. H., Cormier-Daire, V., Hall, C., Krakow, D., Mundlos, S., Nishimura, G., Robertson, S., Sangiorgi, L., Savarirayan, R., Sillence, D., Superti-Furga, A., Unger, S., & Warman, M. L. (2019). Nosology and classification of genetic skeletal disorders: 2019 revision. *American Journal of Medical Genetics. Part A*, *179*(12), 2393–2419. https://doi.org/10.1002/ajmg.a.61366

Mumm, S., Wenkert, D., Zhang, X., McAlister, W. H., Mier, R. J., & Whyte, M. P. (2007). Deactivating germline mutations in LEMD3 cause osteopoikilosis and Buschke-Ollendorff syndrome, but not sporadic melorheostosis. *Journal of Bone and Mineral Research*, *22*(2), 243–250. https://doi.org/10.1359/jbmr.061102

Murphy, M., Kearns, S., Cavanagh, M., O'Connell, D., & Hurson, B. (2003). Occurrence of osteosarcoma in a melorheostotic femur. *Irish Medical Journal*, *96*(2), 55–56 https://www.ncbi.nlm.nih.gov/pubmed/12674159

Rhys, R., Davies, A. M., Mangham, D. C., & Grimer, R. J. (1998). Sclerotome distribution of melorheostosis and multicentric fibromatosis. *Skeletal Radiology*, *27*(11), 633–636. https://doi.org/10.1007/s002560050449

Smith, G. C., Pingree, M. J., Freeman, L. A., Matsumoto, J. M., Howe, B. M., Kannas, S. N., Pyfferoen, M. D., Struss, L. T., Wenger, D. E., Amrami, K. K., Matsumoto, M., & Jurisson, M. L. (2017). Melorheostosis: A retrospective clinical analysis of 24 patients at the Mayo Clinic. *PM & R: The Journal of Injury, Function, and Rehabilitation*, *9*(3), 283–288. https://doi.org/10.1016/j.pmrj.2016.07.530

Vivekanandhan, S., & Mukhopadhyay, D. (2019). Genetic status of KRAS influences transforming growth factor-beta (TGF-beta) signaling: An insight into Neuropilin-1 (NRP1) mediated tumorigenesis. *Seminars in Cancer Biology*, *54*, 72–79. https://doi.org/10.1016/j.semcancer.2018.01.014

Whyte, M. P., Griffith, M., Trani, L., Mumm, S., Gottesman, G. S., McAlister, W. H., Krysiak, K., Lesurf, R., Skidmore, Z. L., Campbell, K. M., Rosman, I. S., Bayliss, S., Bijanki, V. N., Nenninger, A., van Tine, B., Griffith, O. L., & Mardis, E. R. (2017). Melorheostosis: Exome sequencing of an associated dermatosis implicates postzygotic mosaicism of mutated KRAS. *Bone*, *101*, 145–155. https://doi.org/10.1016/j.bone.2017.04.010

Woolridge, B., Stone, N. C., & Denic, N. (2005). Melorheostosis isolated to the calcaneus: A case report and review of the literature. *Foot & Ankle International*, *26*(8), 660–663. https://doi.org/10.1177/107110070502600814

Wordsworth, P., & Chan, M. (2019). Melorheostosis and Osteopoikilosis: A review of clinical features and pathogenesis. *Calcified Tissue International*, *104*(5), 530–543. https://doi.org/10.1007/s00223-019-00543-y

Wynne-Davies, R., & Gormley, J. (1985). The prevalence of skeletal dysplasias. An estimate of their minimum frequency and the number of patients requiring orthopaedic care. *Journal of Bone and Joint Surgery. British Volume (London)*, *67*(1), 133–137. https://doi.org/10.1302/0301-620X.67B1.3155744

Zhang, Y., Castori, M., Ferranti, G., Paradisi, M., & Wordsworth, B. P. (2009). Novel and recurrent germline LEMD3 mutations causing Buschke-Ollendorff syndrome and osteopoikilosis but not isolated melorheostosis. *Clinical Genetics*, *75*(6), 556–561. https://doi.org/10.1111/j.1399-0004.2009.01177.x

How to cite this article: Han, X., Xu, Y., Wei, Z., Wang, C., Yue, H., & Zhang, Z. (2022). Clinical characteristics of 10 Chinese patients with melorheostosis and identification of a somatic MAP2K1 variant in one case. *Molecular Genetics & Genomic Medicine*, *10*, e2043. https://doi.org/10.1002/mgg3.2043